

SHaRe-RL: Structured, Interactive Reinforcement Learning for Contact-Rich Industrial Assembly Tasks

Jannick Stranghöner¹, Philipp Hartmann¹, Marco Braun², Sebastian Wrede^{1,2}, Klaus Neumann^{1,2}

Abstract—High-mix low-volume (HMLV) industrial assembly, common in small and medium-sized enterprises (SMEs), requires the same precision, safety, and reliability as high-volume automation while remaining flexible to product variation and environmental uncertainty. Current robotic systems struggle to meet these demands. Manual programming is brittle and costly to adapt, while learning-based methods suffer from poor sample efficiency and unsafe exploration in contact-rich tasks. To address this, we present SHaRe-RL, a reinforcement learning framework that leverages multiple sources of prior knowledge. By (i) structuring skills into manipulation primitives, (ii) incorporating human demonstrations and online corrections, and (iii) bounding interaction forces with per-axis compliance, SHaRe-RL enables efficient and safe online learning for long-horizon, contact-rich industrial assembly tasks. Experiments on the insertion of industrial Harting connector modules with 0.2–0.4 mm clearance demonstrate that SHaRe-RL achieves reliable performance within practical time budgets. Our results show that process expertise, without requiring robotics or RL knowledge, can meaningfully contribute to learning, enabling safer, more robust, and more economically viable deployment of RL for industrial assembly. Source code and demonstration videos are available at: <https://share-rl.github.io/share-rl.io/>

I. INTRODUCTION

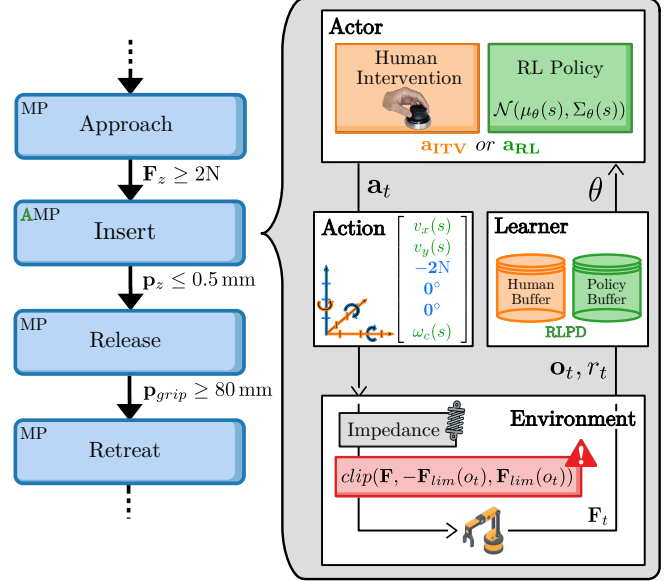
High-mix low-volume (HMLV) industrial assembly, which is ubiquitous in small and medium-sized enterprises (SMEs), remains one of the most difficult challenges for autonomous robots [1]. These settings demand near-zero failure rates, high precision across diverse product variants, and strict compliance with safety regulations, all while operating under inherent environmental uncertainty [2], [3]. The challenge is exacerbated by the fact that SMEs typically lack automation experts, yet depend on production flexibility to remain competitive. Consequently, such tasks are still carried out almost exclusively by human operators. Growing labor shortages further intensify the need for robots that can adapt to changing assembly requirements, but today’s industrial systems remain notoriously inflexible.

Reinforcement learning (RL) promises adaptable robots that can handle uncertainty and even outperform hand-designed controllers or teleoperation [4]. However, deploying RL in real-world industrial settings remains difficult due to sample inefficiency, brittle or engineered reward functions, and the risks of unsafe exploration in contact-rich interactions [5], [6].

*This work was supported by the Fraunhofer Internal Programs under Grant No. SME 40-09551.

¹CITEC, Faculty of Technology, Bielefeld University, Germany.

²Fraunhofer IOSB-INA, Lemgo, Germany.



Structured, Human-in-the-Loop, Real-World RL

Fig. 1: **System overview of SHaRe-RL.** Structure (blue), interaction (yellow), and safety (red) combine to make industrial RL both practical and reliable.

In order to close this gap, prior work has emphasized the importance of injecting domain knowledge into RL [7]. Notably, two powerful forms of prior knowledge commonly exist in industrial settings: process structure, captured by production experts during engineering time through established formalisms [8], and operator expertise, provided through demonstrations and online corrections [9]. Each of these has proven effective in isolation [3], [10], but they have not been combined with modern, sample-efficient RL under real-world safety constraints.

We present SHaRe-RL, a Structured, Human-in-the-loop, and Real-world reinforcement learning framework that integrates these sources of prior knowledge with a simple but effective compliance mechanism. Fig.1 illustrates how SHaRe-RL embeds sample-efficient, interactive RL (green, yellow) within established task abstractions such as MP-Nets (blue), while ensuring safety through adaptive force limits (red). SHaRe-RL scales to complex, vision-based assembly by guiding exploration to meaningful subspaces and focus learning where it is most beneficial. Through demonstrations and online corrections, SHaRe-RL exploits operator expertise to accelerate exploration, while RL itself

is able to improve beyond suboptimal human behavior. This hybrid approach preserves interpretability, supports effective human-robot collaboration, and enables faster, safer, and more economically viable training, moving RL a step closer to broad industrial acceptance. Our contributions are as follows:

- We introduce SHaRe-RL as the first system to combine manipulation primitive nets with human-in-the-loop, off-policy reinforcement learning.
- We formulate an adaptive per-axis compliance mechanism that provably bounds interaction forces during exploration while preserving free-space dynamics.
- We demonstrate empirically that SHaRe-RL achieves robust performance on a sparse-reward industrial insertion task with sub-millimeter tolerances within three hours of real-world interaction, even surpassing the cycle time of a skilled human demonstrator.
- We provide ablations and analysis showing that all components of SHaRe-RL are necessary to succeed in this setting.

II. RELATED WORK

Contact-rich assembly is difficult to solve end-to-end with reinforcement learning, as large state-action spaces, sample efficiency, and strict safety constraints hinder direct trial-and-error learning [2]. Robotics has therefore long relied on abstractions to manage complexity, such as manipulation primitives (MPs) and the Task Frame Formalism [11], [12]. These abstractions can be composed into higher-level structures called Manipulation Primitive Nets (MP-Nets) [8]. Early formulations that combine abstractions with learning-based methods treat primitives as discrete choices with small parameter sets to be optimized [13], [14]. Their process-level coordination can also be learned via hierarchical RL [15]. More recent approaches explore neural-network based primitives, first in isolation for compliant skills such as cutting [16], and later within assembly sequences [3]. While these approaches demonstrate that task structure can drastically reduce exploration complexity, they typically assume on-policy updates, low-dimensional state features and carefully engineered reward functions. This limits their applicability to realistic industrial tasks with high-dimensional input and sparse rewards.

In parallel, advances in sample-efficient RL have shown that offline demonstrations and online interventions can drastically accelerate learning [4]–[6]. Off-policy RL with demonstrations [4], [17], [18], model-based approaches [19], [20], interactive or residual imitation learning [21]–[23], and distributed frameworks like SERL [24] and HIL-SERL [10] demonstrate that human input can turn sparse-reward tasks into tractable real-world learning problems. However, in industrial assembly these methods rarely exploit the forms of prior knowledge that are widely available in practice, and are typically trained and evaluated as isolated skills rather than as components of larger assembly sequences. Our contribution is to embed sample-efficient, human-in-the-loop RL directly into structured assembly processes.

Traditional control approaches often achieve robustness but remain conservative and depend heavily on engineering expertise [25], whereas learning-based controllers promise greater adaptability but face challenges in safety and interpretability. Here, classical optimization-based safety layers, such as control barrier functions (CBFs), quadratic program (QP) filters, and model predictive control (MPC) shields, can enforce constraints during execution, but trade off model accuracy against computational overhead [26]–[28]. Recent work instead learns variable-compliance schemes that adapt robot stiffness through RL, but lower stiffness alone cannot prevent unbounded contact forces when the policy issues large set-points, requiring careful tuning to avoid [29]–[31]. In contrast, deterministic schemes that directly expose physically meaningful limits offer interpretability and ease of deployment. Our method contributes to this line by introducing per-axis adaptive force limits, which provably bound contact forces while preserving free-space dynamics, enabling RL to train safely in contact-rich settings.

III. METHOD

SHaRe-RL combines three complementary sources of domain knowledge into one asynchronous learning pipeline. In this section we first show how human demonstrations and real-time operator interventions are incorporated into an off-policy RL backbone; we then explain how task-frame manipulation primitives focus exploration on the phases that matter most; and we conclude with a simple yet provably safe compliance layer that bounds interaction forces.

A. Operator Guidance: Human-in-the-Loop RL

Robotic reinforcement learning tasks can be formulated as a finite-horizon Markov Decision Process (MDP) where the objective is to learn a policy which maximizes the expected sum of discounted future rewards [32]. Our implementation closely follows the distributed HIL-SERL framework [10], which has proven effective for real-world RL with sparse rewards.

Before training begins, a skilled operator collects a set of teleoperated trajectories with a six-DoF SpaceMouse, which are stored in a demonstration buffer. During training, the operator can press a button to take control of the robot at any time. The policy action is then replaced by the human SpaceMouse action for the duration of the intervention. This enables the operator to bias the dataset toward successful behaviors, help the policy overcome poor local optima and prevent undesirable or unsafe states [10]. Beyond corrections, the operator can also deliberately induce rare but relevant failure cases, forcing the policy to learn robust recovery behavior. In practice, operators intervene frequently during the early stages of training and reduce their involvement as performance improves, with faster convergence when corrections are short and specific while otherwise letting the policy explore on its own.

At the system level, an actor process executes the current policy on the robot, generates experience, and streams it to the learner. The learner process samples mini-batches

equally from the demonstration buffer and an on-policy buffer to performs gradient updates on the RLPD loss [18]. RLPD is a regularized variant of SAC [33] designed for sample efficiency and integration of prior data without offline pretraining. Updated network weights are streamed back to the actor at fixed time intervals.

B. Task-Level Priors: TFF and MP-Nets

Human-in-the-loop corrections alone are not sufficient to enable long-horizon assembly, as the search space quickly becomes intractable without additional structure. A widely used strategy in robotics is to decompose complex processes into manipulation primitives (MPs), each representing a fundamental capability of the manipulator [34]. Finkemeyer et. al [8] formalize MPs as the following tuple

$$\text{MP} := \{\text{HM}, \tau, \lambda\},$$

where HM describes a hybrid force- or position control policy for each translational and rotational direction relative to a task frame, τ is a tool command and λ is a boolean predicate on sensor values that defines a stop condition [11], [12]. Importantly, the type of controller can differ in all directions. Manipulation Primitive Nets (MP-Nets) extend this abstraction by composing MPs into state machines, where transitions are triggered by stop conditions [8], an example of which is given in Fig. 4.

Classical MPs are executed with fixed control setpoints. Extending this notion, adaptive MPs (AMPs) replace selected setpoints by policy-controlled variables [3]. If n axes are controlled by the policy, the corresponding action space is n -dimensional. The operator’s SpaceMouse is likewise constrained to these n axes, ensuring that both demonstrations and interventions remain aligned with the degrees of freedom available to the policy. This formulation focuses exploration on task-relevant directions and high-reward regions of the state-space. For example, in peg-in-hole insertion, the coarse approach is executed with fixed setpoints, while learning is reserved to handle uncertainty during fine alignment.

SHAR-RL uses end-to-end demonstrations as a complementary source of prior knowledge to improve the sample efficiency of AMPs. Instead of training individual MPs in isolation with their own reset strategy, both demonstrations and online rollouts traverse the entire MP-Net from initial to terminal state. During data collection the operator teleoperates adaptive primitives with the SpaceMouse, while non-adaptive primitives run with fixed set-points; all predefined stop conditions are active. When a stop event is difficult to encode analytically, the operator can signal the end of a primitive with a button press. These labels are used to train a lightweight binary classifier that later triggers the same transition autonomously, which is common practice in real-world RL [35].

This design has three advantages. First, MP-Nets can explicitly encode reset strategies, so the same graph that executes a task also brings the system back to a well-defined start state. This makes MP-Nets a naturally formalism for reset-free RL [36]. Second, multiple adaptive primitives can

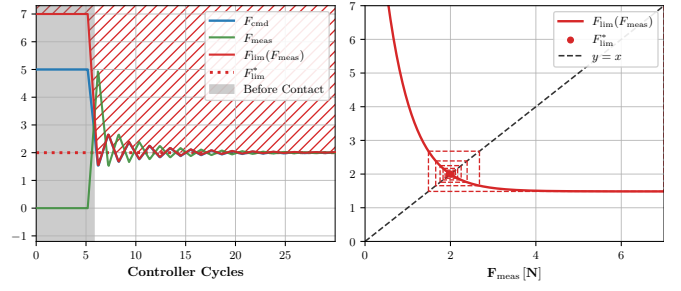


Fig. 2: **Adaptive force limits under ideal conditions** Left: Time response of a stable adaptive limit. Right: Phase-plane cobweb plot illustrating the recurrence in Eq.2.

be optimized concurrently, which eases the cognitive load on the human operator and reduces overall training time. Third, the initial state distribution of each AMP is correctly induced by its predecessors. Specifically, uncertainty introduced by upstream actions, such as variability in a grasp, must be handled robustly by downstream primitives. Training with “atomic” reset strategies would alter these distributions and yield policies that generalize poorly at execution time. Training with full MP-Net rollouts instead exposes policies to the exact state distributions they will encounter, ensuring robustness during deployment.

C. Adaptive Safety Limits

Exploration in contact-rich assembly can easily produce large, destructive contact forces. Beyond the risk of hardware damage, such events degrade sample efficiency by aborting episodes early and biasing trajectory distributions. To address this, we introduce adaptive per-axis force limits as a deterministic safety layer for compliant control. This mechanism enforces physically meaningful force bounds under contact without compromising responsiveness in free-space.

Let $F_{\text{cmd},t}$ denote the raw output of the high-level controller or policy, and $F_{\text{meas},t}$ the measured contact force at time step t . Given a static hardware bound $F_{\text{max}} > 0$, we define a time-varying adaptive limit

$$F_{\text{lim},t}(F_{\text{meas},t}) = \alpha(|F_{\text{meas},t}|) F_{\text{max}} > F_{\text{cmd},t}, \quad (1)$$

where $\alpha : \mathbb{R}_{\geq 0} \rightarrow (0, 1]$ is a monotone decreasing map with $\alpha(0) = 1$. This limit is large during free-space motion, and contracts once contact is detected ($F_{\text{meas},t} > 0$). Assuming rigid-body contact ($F_{\text{meas},t+1} = F_{\text{cmd},t}$) the closed loop evolves as

$$F_{\text{meas},t+1} = F_{\text{lim},t} = \alpha(F_{\text{meas},t}) F_{\text{max}} \quad (2)$$

The long-term behavior of this recurrence is governed by its fixed point F_{lim}^* , which corresponds to the steady-state force established under contact. Convergence to F_{lim}^* is guaranteed whenever the recurrence is locally stable, i.e., it satisfies

$$|\alpha'(F_{\text{lim}}^*)| F_{\text{max}} < 1 \quad (3)$$

A practical choice for α is an exponential decay with minimal scaling α_{min} :

$$\alpha(F) = \alpha_{\text{min}} + (1 - \alpha_{\text{min}}) \exp(-F/\theta). \quad (4)$$

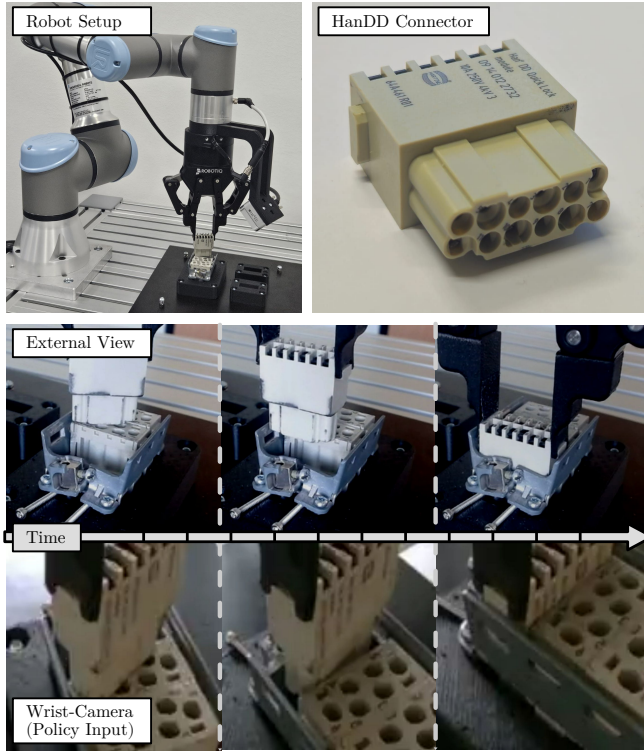


Fig. 3: **Experimental setup and task.** Top: UR3e robot and Harting HanDD industrial connector used for evaluation. Bottom: External view and corresponding policy input over time.

This form is smooth, monotone, and admits a unique fixed point, which can be set by analytically solving for the corresponding decay parameter θ^* . Stability then reduces to a simple inequality on α_{\min} , which is conceptually similar to contraction-based verification of dynamical systems [37]. Fig. 2 illustrates the idealized time and phase-plane response of a stable adaptive force limit. Large commands are allowed in free space, but once F_{meas} exceeds zero the limit shrinks and both commanded and measured forces settle at F_{lim}^* without manual tuning.

IV. CONNECTOR ASSEMBLY TASK

We evaluate our approach on the insertion of industrial Harting Han-Modular connectors, a representative contact-rich assembly task with tolerances of only 0.2–0.4 mm. The task resembles peg-in-hole insertion but involves non-cylindrical geometries and a final snap-in stage. Fig.3 illustrates the task, and Fig. 4 summarizes the relevant manipulation primitives and their configurations. The MP-Net begins with an approach primitive where the connector is already gripped and ends upon contact detection. Then, a single adaptive primitive performs the fine insertion, followed by a snap-in press and a release before retracting. For repeated rollouts during training, the snap-in and release primitives are skipped.

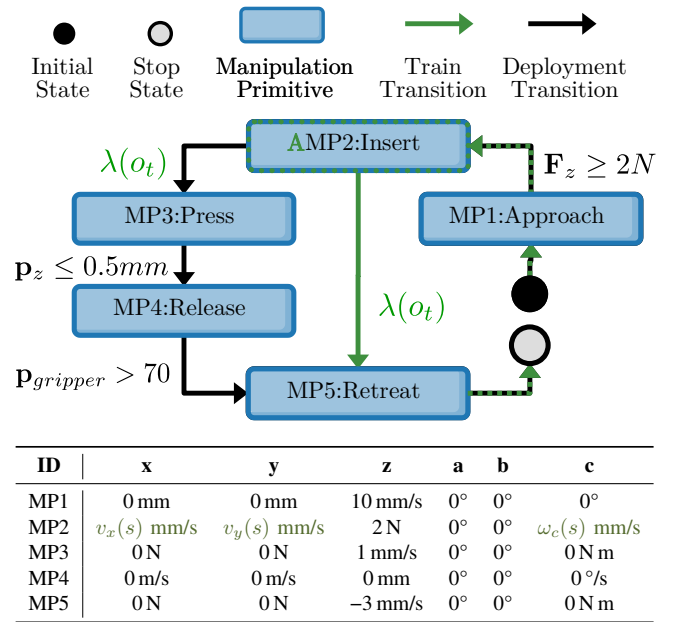


Fig. 4: **MP-Net for the HanDD connector insertion.** The controller setpoints for each direction of the MPs are shown in the table below the diagram. Adaptive MPs, learned stop conditions and variable setpoints are colored green.

A. Robot and Controller

Experiments are conducted on the UR3e depicted in Fig. 3, which is equipped with an integrated six-axis force/torque sensor at the wrist, an ego-centric Intel RealSense D405 RGB-D camera, and custom 3D-printed gripper fingers. The control hierarchy consists of three layers. At the top, desired force or velocity setpoints in task-frame axes are updated at 10 Hz. These targets are processed by a mid-level Cartesian impedance loop running at 500 Hz, which translates them into wrench commands for the robot’s proprietary force controller. This formulation enables to apply adaptive per-axis force limits directly to the commanded wrench before it reaches the hardware. In free space, the maximum limits are set to 7 N for translation and 2 N m for rotation, while under contact the adaptive scaling shrinks to two 2 N and 0.4 N m, respectively, ensuring safety during exploration.

B. MDP Formulation

The connector insertion is modeled as a finite-horizon MDP with observation space

$$o_t = (I_t, \mathbf{x}_{t-1:t}, \mathbf{F}_{t-1:t}), \quad (5)$$

where $I_t \in \mathbb{R}^{128 \times 128 \times 3}$ is the wrist-mounted RGB image, $\mathbf{x}_{t-1:t} \in \mathbb{R}^{2 \times 9}$ are stacked end-effector poses and velocities, and $\mathbf{F}_{t-1:t} \in \mathbb{R}^{2 \times 6}$ are stacked wrenches. Frame stacking compensates for partial observability and non-Markovian effects introduced by the compliant controller. Images are cropped and downsampled to a local view, augmented with random shifts, and encoded with a frozen, pretrained ResNet10 [38], [39]. The resulting embeddings are concatenated with proprioceptive and wrench features

before being processed by policy and critic networks. Both policy and critic are implemented as two-layer multilayer perceptrons (MLPs) with 256 hidden units per layer and SiLU activations [40]. The policy outputs the parameters of a diagonal Gaussian, which is squashed with \tanh to enforce action limits, following the standard practice from Soft Actor-Critic [33].

Compared to prior work, we expose an additional rotational degree of freedom around the connector’s c -axis and increase initial pose uncertainty. At every episode start, the approach pose is perturbed by Gaussian noise in translation ($\sigma_{x,y} = 5$ mm) and orientation ($\sigma_c = 10^\circ$). To simulate systematic calibration errors, the initial distribution is offset by 2 cm along the x -axis. As a result, the policy must traverse a longer distance before fine alignment, increasing the maximum episode length from 3 s to 9 s (90 steps). The action space consists of Cartesian velocity setpoints for the x -, y -, and c -axes. To prevent overfitting to fixed geometry, absolute positions along learned axes are excluded from the state input.

The reward function is either dense, based on vertical distance to the target, or a sparse binary classifier trained from demonstrations:

$$r_t^{\text{dense}} = -\|z_t - z_{\text{goal}}\|_2, \quad r_t^{\text{sparse}} = \lambda(o_t),$$

Since many industrial success signals are inherently sparse, and sparse classifiers tend to generalize better under uncertainty [41], we evaluate on r_t^{sparse} for our main experiments and use r_t^{dense} for ablations.

V. EXPERIMENTAL RESULTS

A key premise of our method is that task-level motion primitives drastically reduce the size of the effective state-action space, and thereby lower the overall complexity of the learning problem. This enables RL to become sample-efficient enough for real-world training. At the same time, this also benefits interactive imitation learning (IL) methods, such as human-gated dataset aggregation (HG-Dagger) [23], by allowing demonstrations to achieve near-complete coverage of primitive-level behavior. As a result, compounding errors are rare and behavior cloning policies remain largely in-distribution during rollouts. Thus, when combining demonstrations with online human corrections, we are faced with a design decision: direct regression onto demonstrations and interventions, as in HG-Dagger, or reinforcement learning accelerated by this data, as in SHaRe. To study this trade-off directly, we compare both under identical human effort, using the same number of demonstrations and the same wall-clock budget.

For consistency, we name all of our structured off-policy RL variants under the SHaRe umbrella. SHaRe (full) denotes the complete system with demonstrations and interventions. SHaRe (no-interventions), SHaRe (no-demos), SHaRe (no-vision), and SHaRe (no-priors) ablate interventions, demonstrations, vision, and task-level priors, respectively. In contrast, PPO and HG-Dagger use a different training loss, and are therefore denoted as PPO (AMP) and HG-Dagger

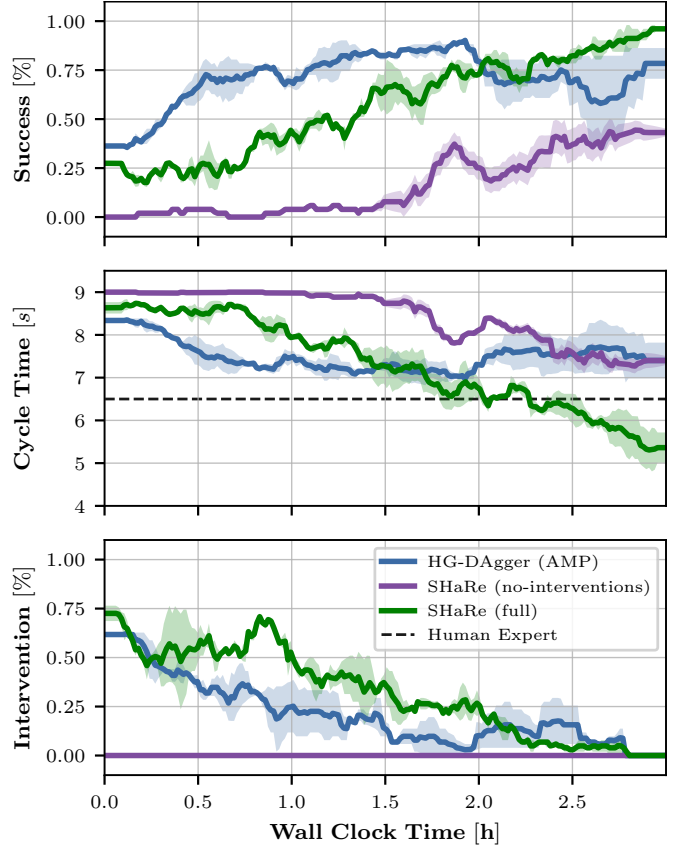


Fig. 5: **Main comparison of learning approaches.** Success rate, cycle time, and intervention rate vs wall-clock time (mean \pm s.e.m., 3 seeds).

(AMP) to emphasize that they still exploit the same primitive structure.

A. Protocol

We compare the performance of each method over three training runs, using a fixed wall-clock budget of three hours on a single NVIDIA RTX 3060 Ti workstation. Each variant is initialized with 20 teleoperated demonstrations and evaluated at the end of training using 20 autonomous rollouts without interventions. During training, success rate, cycle time and intervention rate of the insertion primitive are tracked using a rolling average. The policy executes at 10 Hz; accounting for delays, such as resets or scripted motion, results in an effective environment rate of approximately 6 steps per second.

B. Main Results

Fig. 5 and Table I summarize the main comparison. Among all evaluated methods, SHaRe (full) achieves the highest success rate and the lowest cycle time, even outperforming the human expert baseline. By the end of training, it reaches an average success rate of 95% and completes the insertion task in 5.4 s, compared to 80% and 7.4 s for HG-Dagger, and 6.5 s for the human expert. Despite the disadvantage in raw wall-clock efficiency (HG-Dagger performs

Method	Success [%]	Cycle Time [s]	Human Effort [min]	Updates [$\times 10^3$]	Structure	Demos	Interventions
PPO (AMP)	5	8.8	–	0.5	✓	✗	✗
HG-Dagger (AMP)	80	7.4	5.1	270	✓	✓	✓
SHaRe (no-demos)	35	7.9	–	43	✓	✗	✗
SHaRe (no-interventions)	45	7.5	–	43	✓	✓	✗
SHaRe (no-vision)	10	8.8	12.0	450	✓	✓	✓
SHaRe (no-priors)	5	8.9	–	43	✗	✗	✗
SHaRe (full)	95	5.4	9.7	43	✓	✓	✓
Human Expert	100	6.5	–	–	–	–	–
Random Policy	2	8.9	–	–	–	–	–

TABLE I: Main comparison across methods. SHaRe variants share the same off-policy RL backbone but differ in which sources of prior knowledge are used. PPO and HG-Dagger use different update rules and are therefore denoted with the suffix (AMP), indicating that they still exploit the task-level primitive structure.

roughly 6x more gradient steps), SHaRe outperforms HG-Dagger by learning more robust and time-optimal behaviors. This is most evident during later stages of training: while HG-Dagger improves quickly, it plateaus near the quality of its demonstrations, whereas SHaRe continues to improve throughout the full training budget.

This reflects the core strengths of reinforcement over imitation learning. Human demonstrations can be suboptimal due to pauses, conservative behavior or operator tendencies. For example, we observed that humans typically align each axis sequentially when using a spacemouse, resulting in longer trajectories. IL is asymptotically bounded by such suboptimality, while RL can utilize dynamic programming to learn from both successes and failures. This allows SHaRe to self-correct, discover behaviors that are hard to demonstrate, such as simultaneous multi-axis alignment with optimal dynamics, and ultimately exceed human performance. These findings are consistent with theoretical results from Luo et al. [42], who show that RL can asymptotically outperform IL when human corrections are suboptimal.

We also evaluate intervention rates during training to measure the shift toward autonomous execution. Specifically, we compute the ratio of intervened timesteps to total timesteps per episode, averaged over a 20-episode window. As shown in Fig. 5, SHaRe’s reliance on human corrections steadily decreases and reaches zero by the end of training. Qualitatively, we observe a shift from long, sparse interventions early in training to brief, targeted corrections as the policy matures.

Finally, we evaluate SHaRe (no-interventions), which includes demonstrations but excludes online corrections. This variant plateaus at around 40% success, confirming that demonstrations alone are insufficient under the large pose uncertainties considered. Without interventions, the policy often hesitates in challenging initializations and fails to improve beyond partial success.

C. Ablation Study

The ablations in Table I disentangle the contributions of prior knowledge and sensor modalities. PPO (AMP), relying only on uninformed Gaussian exploration, reaches just 5% success after the full training budget, highlighting its inability to handle sparse reward and vision input. Off-policy RL

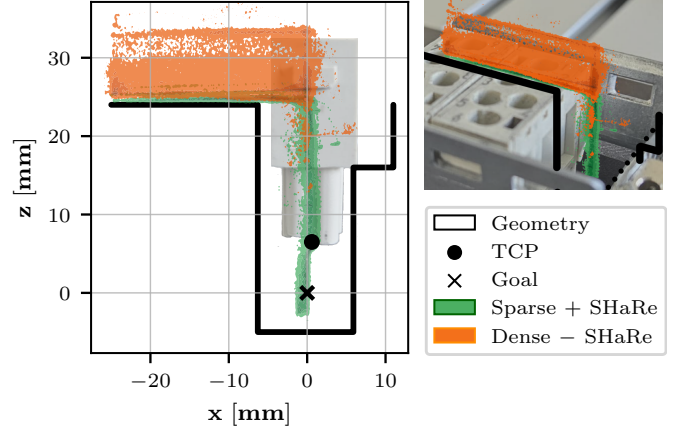


Fig. 6: State-space occupancy during training. Fully autonomous rollouts projected onto a 2D x - z slice of the workspace. Without SHaRe, trajectories remain above the opening and rarely enter the narrow funnel, even though the reward is dense. With SHaRe, occupancy concentrates in goal-relevant regions.

without demonstrations, SHaRe (no-demos), improves to 35%, suggesting that entropy-driven exploration helps but remains insufficient.

Removing image observations (SHaRe no-vision) reduces performance to 10%. The task requires resolving geometric ambiguity in the connector’s c -axis, which cannot be inferred reliably from force and velocity alone. This result supports our design choice to incorporate visual feedback, as richer modalities become essential when uncertainty is high.

Finally, SHaRe (no-priors) replaces the sparse binary reward with a dense shaping reward based on z -axis distance, while simultaneously removing all forms of prior knowledge. In particular, the constant downward force and the manual approach primitive are eliminated, such that the policy must also control the z -axis directly rather than taking over only after contact. Despite the continuous rewards when moving downward, this variant performs worst. The policy fails to align the connector reliably, as the reward landscape is largely flat along rotational axes.

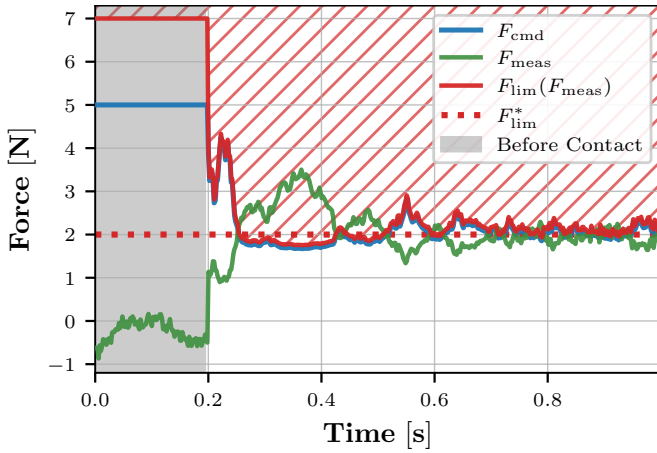


Fig. 7: **Adaptive force limits on the real system.** Commanded vs measured F_z during insertion. Free space (grey) allows large commands; upon contact, limits contract and measured forces converge to the designed equilibrium F_{lim}^* .

D. Analysis

To better understand the role of task and operator priors, we visualize the occupancy distribution of end-effector states during training in Fig. 6. Here, we compare strictly autonomous rollouts of our best-performing SHaRe (full) agent to the SHaRe (no-priors) ablation in which the policy is trained with a dense shaping reward but without any task-level priors or human guidance. The state occupancy is projected onto the x - z cross-section of the insertion task workspace, where lower z values correspond to deeper insertions and thus higher dense reward. Importantly, these regions are only accessible when the connector is properly aligned along all controlled axes. The dense-reward ablation, lacking demonstrations and interventions, explores a much larger state space due to the added degree of freedom and absence of operator corrections. However, uncertainty in hole orientation renders the dense reward largely uninformative for alignment. As a result, most trajectories remain centered above the opening and rarely enter the narrow funnel that leads to successful insertion. In contrast, SHaRe concentrates much of its occupancy in the lower region of the state space, despite relying solely on sparse binary rewards. This confirms that well-chosen priors can be more effective than hand-crafted shaping rewards for guiding exploration in sparse-reward industrial assembly.

We also analyze our adaptive safety limits by measuring commanded and measured z -axis forces during insertion, which is depicted in Fig. 7. Before contact, the controller allows large commanded forces, enabling fast and decisive free-space motion. Upon contact, the limits are adaptively reduced, stabilizing the measured force at the desired equilibrium. Despite significant sensor noise of ± 2 N, transient peaks dampen quickly, ensuring bounded contact forces even during aggressive exploration. With adaptive limits, human teleoperators achieved a 6.5 s average cycle time at 100% success over 50 trials. By contrast, imposing the equilibrium

force as a static hard limit increases the cycle time to 8.7 s and reduces success to 78%. Thus, adaptive limits not only protect hardware, but also directly improve learning efficiency.

VI. CONCLUSION

This work introduced SHaRe-RL, a modular and generally applicable reinforcement learning framework that shows how structured knowledge and interactive learning together overcome the limitations of both hand-engineered control and pure learning-based methods. Our results suggest that, when guided by domain expertise already present in SMEs, RL can be both sample-efficient and safe enough for practical use, which substantially lowers the barrier to deploying learning in contact-rich industrial assembly.

A key challenge that remains is the amount of human supervision required for complex tasks. This motivates future work on more autonomous methods, such as model-based exploration [43], or self-supervised reward signals from images [44]. Our method is also orthogonal to other means of reducing real-world training time, such as offline RL pretraining [45], sim-to-real transfer [46], and the integration of large datasets and pretrained models [47].

Looking ahead, several directions appear promising. Extending SHaRe-RL to longer-horizon assembly processes with multiple adaptive primitives would test its scalability beyond single insertion tasks. Generalization across connector types, geometrical variations, and part tolerances remains an important step toward industrial robustness. Integration with higher-level planning tools, for instance linking CAD models to automatically generated MP-Nets, could further reduce engineering overhead.

REFERENCES

- [1] A. Peterson, “High-Mix/Low-Volume Manufacturers Are a Sweet Spot for Collaborative Robots,” *NIST*, Jul. 2020.
- [2] Í. Elguea-Aguinaco *et al.*, “A review on reinforcement learning for contact-rich robotic manipulation tasks,” *Robotics and Computer-Integrated Manufacturing*, vol. 81, p. 102517, Jun. 2023.
- [3] M. Braun and S. Wrede, “Grey-Box Learning of Adaptive Manipulation Primitives for Robotic Assembly,” in *2023 IEEE International Conference on Robotics and Automation (ICRA)*, May 2023, pp. 12 381–12 387.
- [4] A. Rajeswaran *et al.*, “Learning Complex Dexterous Manipulation with Deep Reinforcement Learning and Demonstrations,” Jun. 2018.
- [5] M. Vecerik *et al.*, “Leveraging Demonstrations for Deep Reinforcement Learning on Robotics Problems with Sparse Rewards,” Oct. 2018.
- [6] J. Luo *et al.*, “Deep Reinforcement Learning for Robotic Assembly of Mixed Deformable and Rigid Objects,” in *2018 IEEE/RSJ International Conference on Intelligent Robots and Systems (IROS)*, Oct. 2018, pp. 2062–2069.
- [7] M. Braun and S. Wrede, “Incorporation of Expert Knowledge for Learning Robotic Assembly Tasks,” in *2020 25th IEEE International Conference on Emerging Technologies and Factory Automation (ETFA)*, vol. 1, Sep. 2020, pp. 1594–1601.
- [8] B. Finkemeyer, T. Kröger, and F. M. Wahl, “Executing assembly tasks specified by manipulation primitive nets,” *Advanced Robotics*, vol. 19, no. 5, pp. 591–611, Jan. 2005.
- [9] H. Beierling *et al.*, “Advancing human-robot collaboration: The impact of flexible input mechanisms,” in *Mechanisms for Mapping Human Input to Robots From Robot Learning to Shared Control/Autonomy-Workshop RSS*, vol. 2024, 2024.
- [10] J. Luo *et al.*, “Precise and Dexterous Robotic Manipulation via Human-in-the-Loop Reinforcement Learning,” Oct. 2024.

- [11] M. T. Mason, "Compliance and Force Control for Computer Controlled Manipulators," *IEEE Transactions on Systems, Man, and Cybernetics*, vol. 11, no. 6, pp. 418–432, Jun. 1981.
- [12] T. Kroger, B. Finkemeyer, and F. Wahl, "A task frame formalism for practical implementations," in *IEEE International Conference on Robotics and Automation, 2004. Proceedings. ICRA '04. 2004*, vol. 5, Apr. 2004, pp. 5218–5223.
- [13] W. Masson, P. Ranchod, and G. Konidaris, "Reinforcement Learning with Parameterized Actions," Nov. 2015.
- [14] M. Dalal, D. Pathak, and R. Salakhutdinov, "Accelerating Robotic Reinforcement Learning via Parameterized Action Primitives," Oct. 2021.
- [15] N. Vuong and Q.-C. Pham, "Reinforcement Learning with Parameterized Manipulation Primitives for Robotic Assembly," Jun. 2023.
- [16] A. Padalkar *et al.*, "Learning to Close the Gap: Combining Task Frame Formalism and Reinforcement Learning for Compliant Vegetable Cutting," in *Proceedings of the 17th International Conference on Informatics in Control, Automation and Robotics, ICINCO 2020, July 7-9, 2020*. SciTePress, Science and Technology Publications, Jul. 2020, pp. 221–231.
- [17] H. Hu, S. Mirchandani, and D. Sadigh, "Imitation Bootstrapped Reinforcement Learning," May 2024.
- [18] P. J. Ball *et al.*, "Efficient Online Reinforcement Learning with Offline Data," May 2023.
- [19] A. Nagabandi *et al.*, "Learning to Adapt in Dynamic, Real-World Environments Through Meta-Reinforcement Learning," Feb. 2019.
- [20] P. Wu *et al.*, "DayDreamer: World Models for Physical Robot Learning," Jun. 2022.
- [21] L. Ankile *et al.*, "From Imitation to Refinement – Residual RL for Precise Assembly," Nov. 2024.
- [22] S. Ross, G. J. Gordon, and J. A. Bagnell, "A Reduction of Imitation Learning and Structured Prediction to No-Regret Online Learning," Mar. 2011.
- [23] M. Kelly *et al.*, "HG-Dagger: Interactive Imitation Learning with Human Experts," Mar. 2019.
- [24] J. Luo *et al.*, "SERL: A Software Suite for Sample-Efficient Robotic Reinforcement Learning," Feb. 2024.
- [25] P. Hartmann, J. Stranghöner, and K. Neumann, "End-to-End Low-Level Neural Control of an Industrial-Grade 6D Magnetic Levitation System," <https://arxiv.org/abs/2509.01388v1>, Sep. 2025.
- [26] Y. Meng *et al.*, "ConBaT: Control Barrier Transformer for Safe Policy Learning," Mar. 2023.
- [27] G. Dalal *et al.*, "Safe Exploration in Continuous Action Spaces," Jan. 2018.
- [28] X. Wang *et al.*, "Guarding Force: Safety-Critical Compliant Control for Robot-Environment Interaction," May 2024.
- [29] A. B. Tahmaz, R. Prakash, and J. Kober, "Impedance Primitive-augmented Hierarchical Reinforcement Learning for Sequential Tasks," Aug. 2025.
- [30] C. C. Beltran-Hernandez, I. G. Ramirez-Alpizar, and K. Harada, "Variable Compliance Control for Robotic Peg-in-Hole Assembly: A Deep Reinforcement Learning Approach," *Applied Sciences*, vol. 10, no. 19, p. 6923, Oct. 2020.
- [31] R. Martín-Martín *et al.*, "Variable Impedance Control in End-Effector Space: An Action Space for Reinforcement Learning in Contact-Rich Tasks," Aug. 2019.
- [32] R. S. Sutton and A. G. Barto, *Reinforcement Learning: An Introduction*, second edition ed., ser. Adaptive Computation and Machine Learning Series. Cambridge, Massachusetts: The MIT Press, 2018.
- [33] T. Haarnoja *et al.*, "Soft Actor-Critic: Off-Policy Maximum Entropy Deep Reinforcement Learning with a Stochastic Actor," Aug. 2018.
- [34] F. Suárez-Ruiz and Q. C. Pham, "A Framework for Fine Robotic Assembly," Sep. 2015.
- [35] A. Singh *et al.*, "End-to-End Robotic Reinforcement Learning without Reward Engineering," May 2019.
- [36] A. Gupta *et al.*, "Reset-Free Reinforcement Learning via Multi-Task Learning: Learning Dexterous Manipulation Behaviors without Human Intervention," in *2021 IEEE International Conference on Robotics and Automation (ICRA)*, May 2021, pp. 6664–6671.
- [37] K. Neumann and J. J. Steil, "Learning robot motions with stable dynamical systems under diffeomorphic transformations," *Robotics and Autonomous Systems*, vol. 70, pp. 1–15, Aug. 2015.
- [38] N. Hansen and X. Wang, "Generalization in Reinforcement Learning by Soft Data Augmentation," Apr. 2021.
- [39] K. He *et al.*, "Deep Residual Learning for Image Recognition," Dec. 2015.
- [40] S. Elfving, E. Uchibe, and K. Doya, "Sigmoid-Weighted Linear Units for Neural Network Function Approximation in Reinforcement Learning," Nov. 2017.
- [41] G. Schoettler *et al.*, "Deep Reinforcement Learning for Industrial Insertion Tasks with Visual Inputs and Natural Rewards," Aug. 2019.
- [42] B. Luo *et al.*, "Human-in-the-Loop Reinforcement Learning in Continuous-Action Space," *IEEE Transactions on Neural Networks and Learning Systems*, vol. 35, no. 11, pp. 15 735–15 744, Nov. 2024.
- [43] N. Watters *et al.*, "COBRA: Data-Efficient Model-Based RL through Unsupervised Object Discovery and Curiosity-Driven Exploration," Aug. 2019.
- [44] Y. J. Ma *et al.*, "VIP: Towards Universal Visual Reward and Representation via Value-Implicit Pre-Training," Mar. 2023.
- [45] A. Nair *et al.*, "Learning on the Job: Self-Rewarding Offline-to-Online Finetuning for Industrial Insertion of Novel Connectors from Vision," Feb. 2023.
- [46] L. Bergmann *et al.*, "Precision-Focused Reinforcement Learning Model for Robotic Object Pushing," Nov. 2024.
- [47] O. X.-E. Collaboration *et al.*, "Open X-Embodiment: Robotic Learning Datasets and RT-X Models," Jun. 2024.